Acta Materialia 195 (2020) 571–578

Contents lists available at ScienceDirect

Acta Materialia

journal homepage: www.elsevier.com/locate/actamat

Full length article

Structural evidence for the polymorphic phase boundary in (Na,K)NbO_3 based perovskites close to the rhombohedral-tetragonal phase coexistence zone

Jian Fu, Ruzhong Zuo*

Institute of Electro Ceramics & Devices, School of Materials Science and Engineering, Hefei University of Technology, Hefei 230009, PR China

ARTICLE INFO

Article history:
Received 20 February 2020
Revised 28 May 2020
Accepted 1 June 2020
Available online 10 June 2020

Keywords:
Polymorphic phase boundary
R-T phase boundary
Lead-free
NKN
Thermal instability

ABSTRACT

The multi-phase coexistence is a technologically important concept in high-performance piezoelectric ceramics owing to the ability of achieving extremely increased electromechanical properties. However, in fact it cannot always produce desirable thermal stability of small-field piezoelectric properties relevant to the device application. In this work, a typical lead-free piezoelectric composition of $(Na_{0.52}K_{0.4})(Nb_{0.84}Sb_{0.08})O_3$–0.055$LiTaO_3$–0.025$BaZrO_3$ coexisted with rhombohedral (*R*) and tetragonal (*T*) phases at room temperature was investigated as a case study by means of ex/in-situ synchrotron x-ray diffraction, Rietveld structure refinement and measurements of temperature-dependent electrical properties. The refined crystal structure proves to be a three-phase coexistence of *R*, orthorhombic (*O*) and *T* at virgin state, and evolves into the *R*+monoclinic (M_C)+*T* phase coexistence at poled state owing to an electric field induced irreversible *O*-M_C phase transition. Particularly, the field induced M_C phase can stably exist and maintain its concentration as long as the annealing temperature is below the Curie temperature. An interesting finding is that the poled sample still retains the polymorphism of phase transition like its virgin state featuring the temperature driven *R*-*O*(M_C)-*T* phase transition, leading to seriously degraded piezoelectric coefficients after thermal cycles due to domain de-texturing of not only M_C phase, but also *R* and *T* phases during repeated phase transition. The present study would benefit to understanding of the nature of polymorphic phase boundary and the structure origin of temperature-dependent piezoelectric properties in *R*-*T* coexisted (Na,K)NbO_3-based lead-free solid-solution ceramics.

1. Introduction

Designing a typical phase boundary, which is situated between multiple ferroelectric phases with different symmetries, has played a dominant role in the development of high-performance piezoelectric ceramics [1,2]. Not only domain wall energy is reduced but also the polarization vector can be flexibly rotated via a low-symmetry intermediate phase within the phase coexistence zone, thus leading to significantly enhanced piezoelectric activity [3,4]. A traditional case is the composition driven morphotropic phase boundary (MPB), such as the one between ferroelectric rhombohedral (*R*) -tetragonal (*T*) in virgin Pb(Zr,Ti)O_3 (PZT) or $(Bi_{0.5}Na_{0.5})TiO_3$-$BaTiO_3$ samples [5,6], or the one between ferroelectric orthorhombic O_1-orhombohic O_2 in $NaNbO_3$-$KNbO_3$ (NKN) binary solid solutions [7], which basically corresponds to a nearly vertical region isolating two ferroelectric phases relative to the composition axis. Another typical case, as frequently reported in some lead-free piezoelectric systems such as modified niobate or $BaTiO_3$ systems [8–12], is the composition and temperature driven polymorphic phase boundary (PPB), which was put forward in 2009 to make the difference from the well-known MPB [13], and is characterized by a rather tilting region (or line) separating two ferroelectric phases against the composition axis. The PPB can be usually achieved by shifting different polymorphic phase transition (PPT) temperatures close to room temperature, such as in the *R*-*O* or *O*-*T* coexisted NKN-based ternary or quaternary solid solutions [11,14,15]. Compared with the MPB composition, the PPB composition was reported to usually exhibit serious temperature instability of piezoelectric properties owing to the variation of the phase fraction with temperature [11,13,16–19], largely restricting its possible device applications. That is to say, the physical meaning of phase boundary in piezoelectric ceramics should be renewed by recognizing not only the coexistence of multi ferroelectric phases, but also the phase boundary type, i.e., whether the thermally excited phase transition exists among coexisting ferroelectric phases.

* Corresponding author.
E-mail address: piezolab@hfut.edu.cn (R. Zuo).

https://doi.org/10.1016/j.actamat.2020.06.002
1359-6454/

In recent years, piezoelectric properties have been significantly enhanced in R-T phase coexisted NKN-based perovskite compositions [20–26], since the first work in 2011 [20]. Although these niobate-based lead-free compositions look similar to traditional PZT in terms of the coexisted phase structures (*R* and *T*) at virgin state, there are still some clear differences between them such as *R3c* in the former instead of *R3m* in the latter [27,28], which might contribute differently to the final piezoelectric properties [29]. Moreover, different from the MPB-type PZT system, the *R-T* coexisted NKN-based compositions were reported to still exhibit obvious temperature dependence of small-field electromechanical properties [30–33], as we observed in *R-O* and *O-T* coexisted NKN-based compositions. Accordingly, the nature of the phase boundary between *R* and *T* in virgin or poled NKN-based ceramics needs to be clarified clearly, although the mechanism for high piezoelectric activity for this phase-boundary system has been suggested to be related with an electric field induced intermediate phase [34] or the nanoscale domain morphology [35–38]. In the present study, the $(Na_{0.52}K_{0.4})(Nb_{0.84}Sb_{0.08})O_3$-(0.08-x)$LiTaO_3$-x$BaZrO_3$ ($x = 0.025$, NKNS-LT-0.025BZ) composition, which is located at the crossover between *R* and *T* phases at room temperature [20], was selected as a case study. The structural evidence for the PPB instead of classical MPB determined by clarifying the refined phase structure and its response to electric field and temperature, would explain the complex transitions occurred in the *R-T* coexisted NKN-based system, and consequently, the degradation of its piezoelectric response with subsequent heating treatments.

2. Experimental

The NKNS-LT-0.025BZ ceramic was prepared by a conventional solid-state reaction route. The detailed experimental procedure was reported elsewhere [20]. The two major surfaces of as-sintered ceramics were ground and polished, and then annealed in air at 550 °C for 3 h. Silver pastes were screened on two surfaces and then fired in air at 600 °C for 30 min. Temperature dependent dielectric properties of unpoled and poled samples were measured using an LCR meter (E4980A, Agilent, Santa Clara, CA). The polarization versus electric field (P-E) and strain versus electric field (S-E) curves were measured by using a ferroelectric measuring system (Precision multiferroelectric, Radiant Technologies Inc., Albuquerque, NM) with an accessory laser interferometer vibrometer (AE SP-S 120E, SIOS technic, GmbH, Ilmenau, Germany). The room temperature crystal structure of the ceramic disk or crushed powder under ex-situ and in-situ electric field conditions was examined by synchrotron x-ray diffraction (XRD) at beam line 14B1 at the Shanghai Synchrotron Radiation Facility (SSRF). Both unpoled and poled samples exhibit pure perovskite structure without any secondary phases. For the Rietveld refinement, the XRD pattern of the poled sample was also obtained through grinding the ceramic disk into the powder, just similar to that of the unpoled sample. This way can avoid the preferred orientation effect and help achieve the accurate structure information of the sample. Structural refinement was carried out using the Rietveld refinement program GSAS-II [39]. For in-situ synchrotron XRD measurement, thin gold electrodes were sputtered onto two well-polished surfaces of the ceramic disks, and the sample surface was perpendicular to the applied electric field during the in-situ measurement. Beam energy of 10 keV (λ= 1.2398 Å) were selected and the data were recorded in symmetric reflection geometry with $\theta-2\theta$ step-scans (Bragg-Brentano geometry) using a Huber 5021 six-cycle diffractometer with a NaI scintillation detector. Temperature dependent structure evolution of unpoled and poled samples was characterized by a conventional powder XRD (D/MAX-RB, Rigaku, Tokyo, Japan) using a Cu Kα radiation (λ=1.5406 Å). The slight difference between synchrotron XRD and conventional XRD patterns would be attributed to the different spot size and detection depth between these two x-ray sources, which does not affect the analysis of the phase structure and its evolution. The sample was poled under a dc field of 4 kV/mm at room temperature for 15 min. d_{33} values were measured by using a Belincourt-meter (YE2730A, Sinocera, Yangzhou, China). Samples are open circuited during annealing but short circuited before d_{33} measurement. Before poling, conductive adhesives were screened on two polished surfaces of ceramic discs, then dried at 120 °C. For the temperature dependent XRD measurement, both unpoled and poled samples were in-situ measured using high temperature accessories of XRD. For the thermal annealing measurement, the poled sample was heated from room temperature to a certain temperature, then remained at this temperature for 20 min and finally cooled to room temperature for the d_{33} and XRD measurements.

3. Results

3.1. Refined phase structure of unpoled and poled NKNS-LT-0.025BZ ceramics

The Rietveld refinement was carried out for both unpoled and poled NKNS-LT-0.025BZ ceramic powder by using high-resolution synchrotron XRD data, as shown in Fig. 1. Both samples at room temperature exhibit split and asymmetric $(110)_C$, $(200)_C$ and $(222)_C$ reflections, thus excluding the possibility that only *T* or *R* phase exists. The fitting process of the unpoled sample was initially based on a conventional *R* (*R3c*)+*T* (*P4mm*) two-phase mode, which, however, cannot comfort all peak profiles satisfactorily. Instead, an *R3c* + *Amm2* (*O*) +*P4mm* triple-phase model shows a good agreement between the observed and calculated profiles, as shown in Fig. 1(a). That is to say, the studied sample at virgin state should be composed of *R, O* and *T* phases at room temperature, instead of only two phases of *R* and *T* as early described elsewhere [20]. It should be noted that R3c rather than R3m model was adopted to describe the R because of the existence of tilt-related superstructure (See Supplementary Fig. S1), which can be detected in the single R phase composition with high BZ content. No obvious superstructure can be observed in the $x = 0.025$ sample possibly due to the relatively low R phase content in the currently studied composition, as confirmed by neutron diffraction [27,28]. On the other hand, it can be found that the *R3c*+*Pm*+*P4mm* triple-phase model shows relatively good agreement for the poled sample compared to other models with and/or without lower symmetry phase, such as *R3c*+*P4mm, Cm*+*P4mm, Pm*+*P4mm* two-phase models and even *R3c*+*Cm*+*P4mm* triple-phase mode (See Supplementary Fig. S2). The refined structural parameters of unpoled and poled specimens are given in Table 1. The resulting R_p, R_{wp} and χ^2 listed in Table 1 indicate that the fitting result is satisfactory and reliable for both the unpoled and poled samples. It is evident that electric poling has caused the appearance of a new monoclinic (M_c) phase and the disappearance of initial *O* phase at the same time. This result means that there exists an electric field induced irreversible *O* to M_c phase transition. That is to say, the coexistence of *R, O* and *T* phases at virgin state evolves into the coexistence of *R*, M_c and *T* phase at poled state.

3.2. In-situ electric field dependent phase structure evolution

To further reveal the phase structure change during the poling process, the evolution of $(200)_C$ reflections under different field conditions is shown in Fig. 2. The fitting of the diffraction profiles was carried out by using a pseudo-Voigt peak shape function. The concurrent existence of the $(002)_T/(200)_T$ doublet, $(202)_O/(020)_O$ doublet and $(200)_R$ singlet at $E = 0$ kV/mm further suggests that the unpoled specimen at room temperature should be composed

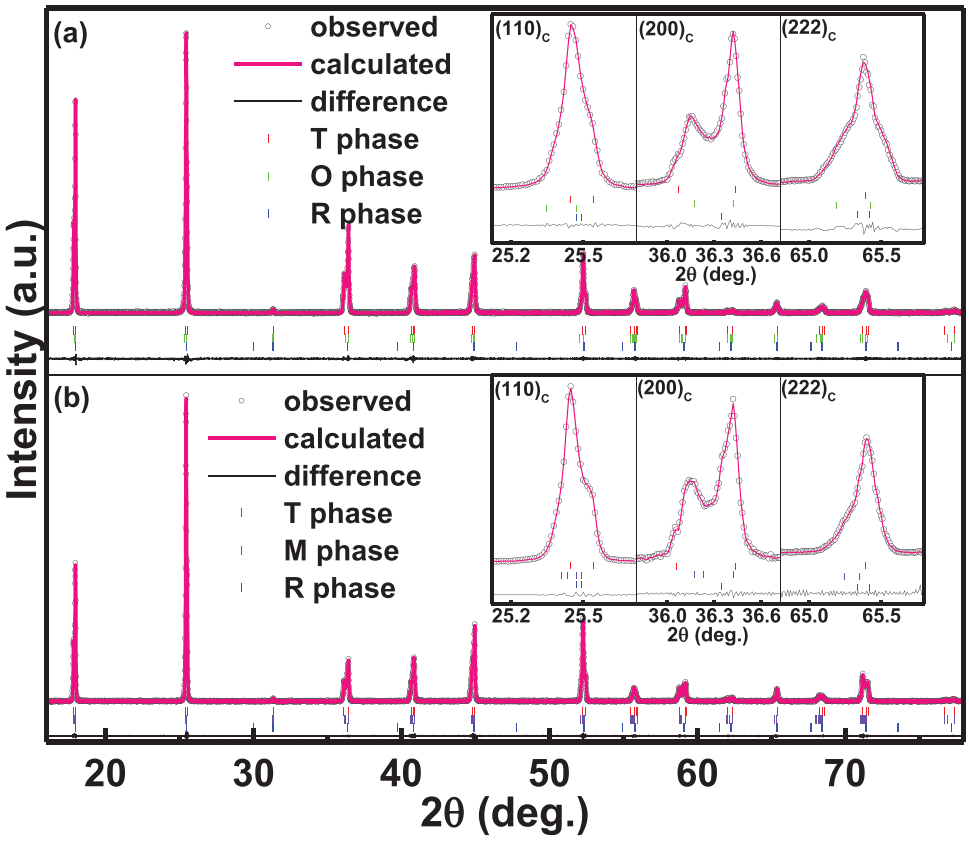

Fig. 1. Rietveld refinement patterns of (a) unpoled and (b) poled NKNS-LT-0.025BZ ceramic powders by means of synchrotron XRD with the wavelength of λ=1.2398 Å. The insets show enlarged profiles of $(110)_C$, $(200)_C$ and $(222)_C$ reflections.

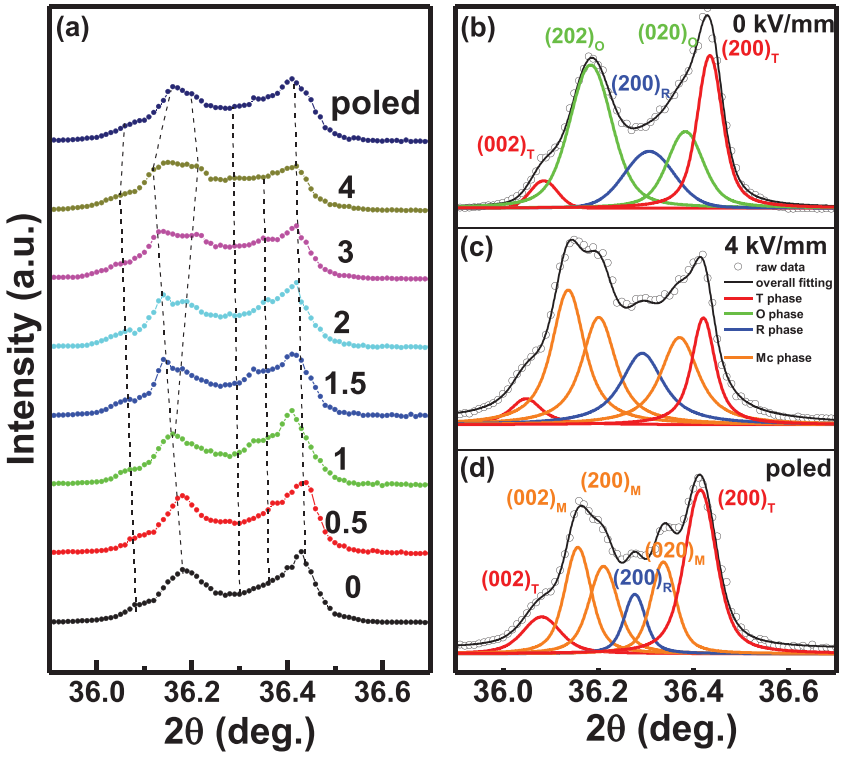

Fig. 2. (a) The evolution of $(200)_C$ reflection of NKNS-LT-0.025BZ ceramic samples under various electric field conditions and the corresponding fitting results of the $(200)_C$ reflection under selected electric field conditions using pseudo-Voigt peak shape function derived from the synchrotron XRD with the wavelength of λ=1.2398 Å: (b) $E = 0$ kV/mm (virgin state), (c) $E = 4$ kV/mm (poling state), and (d) $E = 0$ kV/mm (poled state).

Table 1
Refined structural parameters of the NKNS-LT-0.025BZ ceramic using the *R3c*+*Amm2*+*P4mm* coexisted model for unpoled state and *R3c*+*Pm*+*P4mm* coexisted model for poled state. a, b, c and α are the cell parameters, $U_{iso}$is the isotropic temperature factor, V is the cell volume, profile R-factor (R_p) and weighting profile R-factor (R_{wp}) are the reliability factor and chi squared χ^2 is the goodness-of-fit indicator of fitting.

Unpoled												
Space group	P4mm				Amm2				R3c			
Atoms	x	y	z	U_{iso}(Å^2)	x	y	z	U_{iso}(Å^2)	x	y	z	U_{iso}(Å^2)
Na/K/Li/Ba	0.000	0.000	0.000	0.0093	0.000	0.000	0.000	0.0068	0.000	0.000	0.2919	0.0059
Nb/Sb/Ta/Zr	0.500	0.500	0.507	0.0061	0.500	0.000	0.441	0.0075	0.000	0.000	0.015	0.0102
O1	0.500	0.500	−0.092	0.0058	0.000	0.000	0.416	0.0095	0.750	0.801	0.078	0.0141
O2	0.500	0.000	0.508	0.0113	0.500	0.255	0.24	0.01011				
O3												
Lattice parameters	a = 3.9621(1) Å, c = 3.9912(7) Å, V = 62.656 Å^3, α=β =γ=90°				a = 5.6184(4) Å, b = 3.9640(1) Å, c = 5.6455(2) Å, V = 125.735 Å^3, α=β =γ=90°				a = 5.6142(5) Å, c = 13.7691(7) Å, V = 375.857 Å^3, α=β =90°, γ=120°			
Phase fraction	47.2%				32.9%				19.9%			
R_p=6.8, R_{wp}=4.6, χ^2=2.18												
	poled											
Space group	P4mm				Pm				R3c			
Atoms	x	y	z	U_{iso} (Å^2)	x	y	z	U_{iso} (Å^2)	x	y	z	U_{iso} (Å^2)
Na/K/Li/Ba	0.000	0.000	0.000	0.0085	0.000	0.000	0.000	0.0069	0.000	0.000	0.2901	0.0058
Nb/Sb/Ta/Zr	0.000	0.000	0.512	0.0060	0.550	0.500	0.490	0.0071	0.000	0.000	0.016	0.0097
O1	0.500	0.500	−0.078	0.0047	0.624	0.000	0.511	0.0076	0.746	0.797	0.077	0.0134
O2	0.500	0.000	0.511	0.0112	0.537	0.500	−0.008	0.0122				
O3					0.017	0.500	0.530	0.0143				
Lattice parameters	a = 3.9618(5) Å, c = 3.9915(2) Å, V = 62.650 Å^3, α=β=γ=90°				a = 3.9938(1) Å, b = 3.9732(5) Å, c = 3.9992(2) Å, V = 63.459 Å^3, α=γ=90°, β=90.18°				a = 5.6140(3) Å, c = 13.7685(1) Å, V = 375.804 Å^3, α=β=90°, γ=120°			
Phase fraction	42.6%				41.2%				16.2%			
R_p=7.1, R_{wp}=5.3, χ^2=2.33												

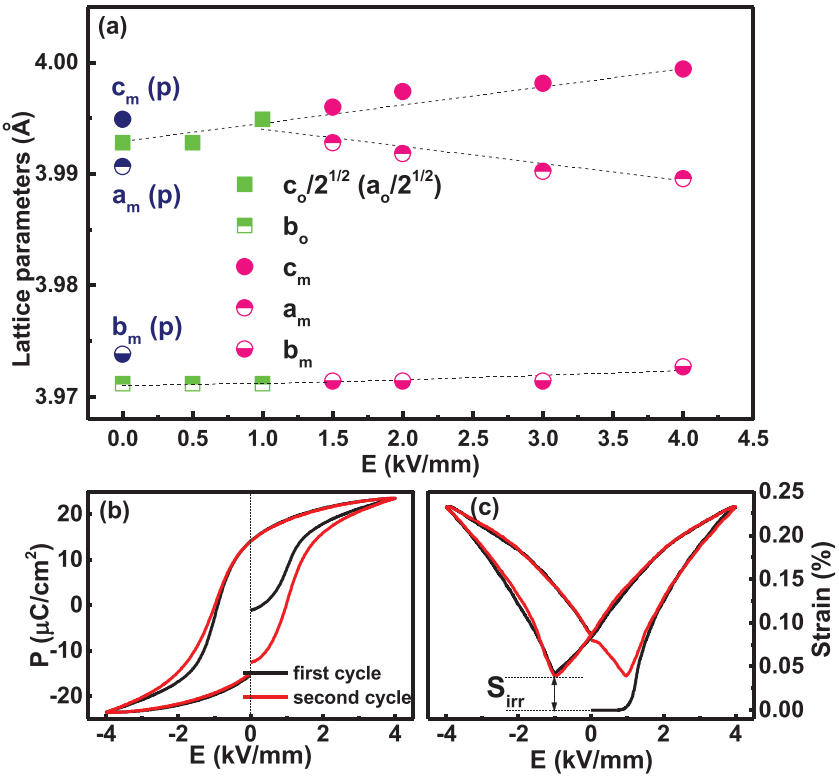

Fig. 3. (a) Evolution of the lattice parameters of *O* and M_C phases during electric field induced irreversible *O* to M_C phase transition, the (b) P-E and (c) S-E curves at different cycles. The subscript p in (a) denotes the poled state.

of three phases *R, O* and *T*. With increasing the electric field amplitude, no obvious change except for a slight change of peak intensity can be observed in both *R* and *T* phases, possibly due to the change of poling texture and the decrease of *R* and *T* phase fraction. However, as $E \geq 1$ kV/mm, an obvious peak splitting from the $(202)_O/(020)_O$ doublet to the $(002)_M/(200)_M/(020)_M$ triplet can be observed. As we know, peak splitting was usually considered as a result of the symmetry lowering into M phase. It is widely accepted that there are two types of M phase, namely monoclinic *Cm* (M_A and M_B) and *Pm* (M_C) as proposed by Vanderbilt et al. [40], in perovskite ferroelectrics. Similar to the *O* phase, the unit cell of *Cm* is double and rotated by 45° around the c axis with respect to the pseudo-cubic cell. However, its polarization vector is not along $[101]_c$ direction, but constrained in the $(10)_c$ plane. The magnitudes of polarization components of *Cm* phase can be thus described as $P_x=P_y\neq P_z$. As a result, only a $(002)_M/(220)_M$ doublet but a $(20)_M/(021)_M/(201)_M$ triplet can be observed for *Cm* symmetry, as evidenced in an *R-O* PPB system [41]. By comparison, the unit cell of *Pm* phase is primitive similar to that of *T* phase, yet its spontaneous polarization P_s is constrained within the $(010)_C$ plane instead of $[001]_C$ axis in *T* phase. As a result, the corresponding polarization components can be described as $P_x\neq P_y\neq P_z$, leading to a $(002)_M/(200)_M/(020)_M$ triplet. The observed $\{200\}_M$ triplet in Fig. 2(c,d) clearly confirms the existence Mc phase rather than M_A phase. This can be also confirmed by the Rietveld refinement of poled ceramic powder as shown in Fig. 1(b) since field induced M_C phase can be maintained even after removal of electric field (Fig. 2(d)).

As derived from in-situ XRD data, the evolution of lattice parameters of *O* and M_C phases with electric field is shown in Fig. 3(a). It can be seen that once M_C phase is induced ($E>1$ kV/mm), c_m and a_m show a slight increase and decrease with increasing electric field, respectively. By comparison, a_m and b_m tend to be close to each other with increasing electric field. This variation tendency would benefit to achieving a continuous rotation of P_s from $[u0w]_C$ ($u\neq w$) to $[001]c$, corresponding to the polarization rotation of M_C phase along the $(010)_C$ plane [5]. It is worthy of note that, although both c_m and a_m show a certain degree of recovery after removal of external electric field, they cannot merge into a single one, suggesting an irreversible *O*-M_C transition during poling process. These changes can be also reflected in polarization versus electric field (P-E) and strain versus electric field (S-E) curves, as shown in Fig. 3(b, c). It can be seen that well-saturated P-E loops can be obtained at both the first and second electric cycles. By comparison, it is worthy of note that the sample exhibits an asymmetric S-E curve with a large strain gap (S_{irr}) on the left side of S-E curve, which transforms into a symmetric one after the first-cycle electric field loading. Interestingly, the value of S_{irr} is just equal to the difference of poling strain between first and second cycles. The observed S_{irr} in poling strains between two cycles should stem from the above-mentioned irreversible phase transition during poling process. Such an irreversible lattice strain of ~0.038% roughly estimated from the equation: $\varepsilon_{irr-lattice} = \frac{d_{(002)M-poled} - d_{(002)O}}{d_{(002)O}}$, shows a good agreement with the observed S_{irr} value (~0.042%). This result further confirms that the new M_C phase should be mainly derived from the initial *O* phase.

3.3. The polymorphism nature of phase boundary

The refined phase structure of this studied phase-boundary composition should also influence its dielectric properties. Fig. 4 shows dielectric properties (permittivity ε_r and loss $\tan\delta$) as well as the evolution of the $(200)_C$ reflection as a function of temperature for unpoled and poled samples. In addition to a distinct dielectric peak near ~180 °C corresponding to their Curie temperatures (T_c), there are still two extra dielectric humps for both cases.

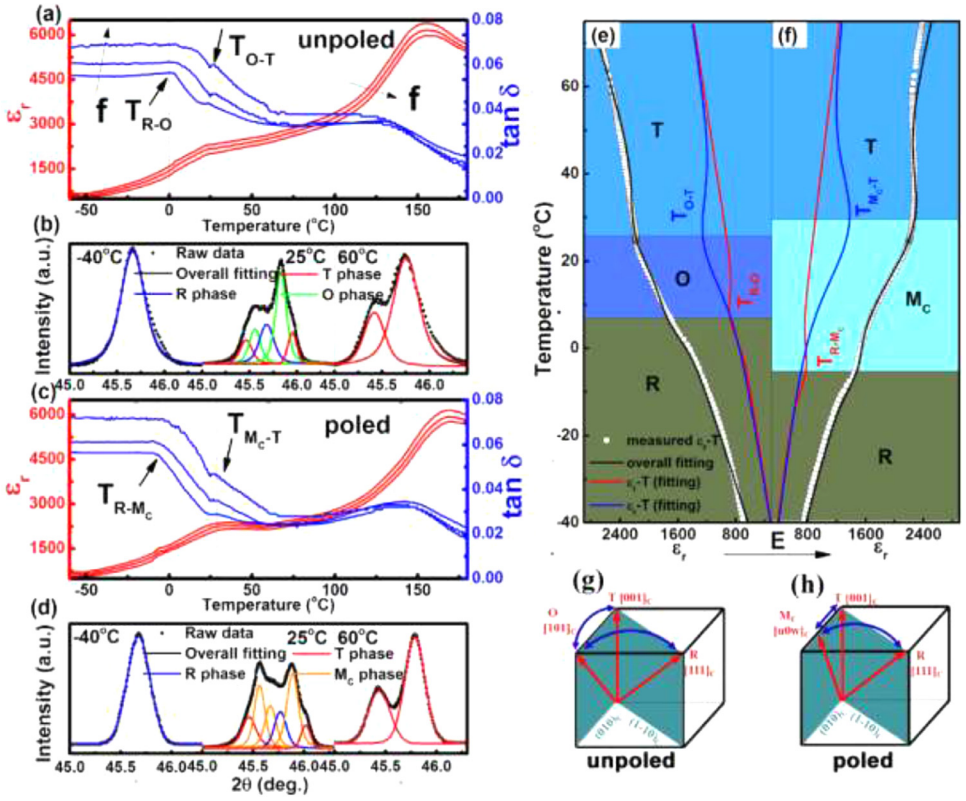

Fig. 4. Temperature dependent dielectric properties in the frequency range of 1–100 kHz and the evolution of $(200)_C$ reflection at selected temperatures fitted by the pseudo-Voigt peak shape function for (a,b) unpoled and (c-d) poled NKNS-LT-0.025BZ ceramics, respectively, derived from the conventional XRD using Cu Kα radiation (λ=1.5406 Å); the deconvolution of dielectric permittivity versus temperature curves of (e) unpoled and (f) poled samples measured at 10 kHz, and the sketch of the polarization rotation path for the studied composition (g) before poling and (h) after poling.

According to the $(200)_c$ diffraction lines at different temperatures (Fig. 4(b)), the phase structure of the unpoled sample changes from a single *R* phase (<~5 °C), to the coexisted $R + O + T$ phase (~5 °C-~25 °C), and then into a single *T* phase (>~25 °C) with increasing temperature in the proximity of room temperature. This indicates that the observed two dielectric humps for the unpoled sample should correspond to the PPT temperatures T_{R-O} and T_{O-T}, respectively (Fig. 4(b)). It is interesting to note that two dielectric anomalies still exist for the poled sample. Based on the temperature dependent XRD data (Fig. 4(d)), the observed two dielectric anomalies after poling should be attributed to the *R*-M_C and M_C-*T* transition, respectively. Particularly, the M_c phase can be maintained in the poled sample, as long as measuring temperature or thermal annealing temperature is not higher than the Curie temperature, although the domain texture degree of M_C phase shows a slight decrease after thermal cycling treatment, as shown in Fig. 5. That is to say, the field induced M_c phase can stably exist in the poled sample, such that the *R*-M_C-*T* transition for the poled sample can be repeatedly driven by temperature, indicating that both *R*-*Mc* and *Mc*-*T* phase transition is polymorphic. This is intrinsically similar to the *R*-*O* and *O*-*T* PPT in the unpoled sample, as shown in Fig. 4(e,f). The triple-phase coexistence of $R + O + T$ or $R+M_C+T$ in the proximity of room temperature (Fig. 4(b, d)) should be attributed to the diffuseness of PPTs, as shown in Fig. 4(e,f). The overlapping of *R*-*O*(M_C) and *O*(M_C)-*T* PPTs leads to a wide dielectric peak around room temperature. This result clearly demonstrates that not only unpoled samples but also poled samples own a PPB, instead of traditional MPB. Moreover, it can be found that electric poling has slightly expanded the temperature zone for the M_c phase by reducing T_{R-Mc} and increasing T_{Mc-T}, compared with T_{R-O} and T_{O-T} values in the unpoled sample. This also interprets why the *R* and *T* phase content at room temperature becomes slightly low after poling (see Table 1). It seems that external electric field helps to stabilize the M_c phase against the *O* phase in the studied sample.

3.4. Thermal instability of d_{33} values

Since the *R*-M_C-*T* transition for the poled sample can be driven by temperature, it should be interesting to explore the temperature dependence of piezoelectric properties induced by PPT upon heating. The d_{33} value was measured at room temperature after annealing at different temperatures for 20 min and then cooled to room temperature. It can be seen from Fig. 6 that static piezoelectric coefficient d_{33} value shows a slight decrease when annealing temperature is below T_c and vanishes rapidly as annealing temperature gets close to T_c. Similar phenomenon can be also observed in O-T and R-O PPB systems [11,13]. In addition, it also can be found from Fig. 6 that the degradation of d_{33} becomes significant with increasing thermal cycling time. After 1st thermal annealing cycle at 60 °C, d_{33} value shows a slight deterioration of ~6.1%. By comparison, it increases up to ~15.1% at 5th cycle. This phenomenon should be attributed to an obvious depolarization from the domain detexturing of M_C phase as well as R and T phases as the poled sample is repeatedly heated across the PPT temperature. This can be confirmed from Fig. 5 that both $002)_T/(200)_T$ and $(002)_M/(200)_M$ intensity ratios decrease from ~1.36 to ~1.29 and ~1.50 to ~1.38 at 1st cycle, respectively, whereas, both values decrease up to ~1.18 and ~1.24 at 5th cycle, suggesting that an obvious depolarization can be observed after thermal annealing, and particularly after repeated thermal annealing.

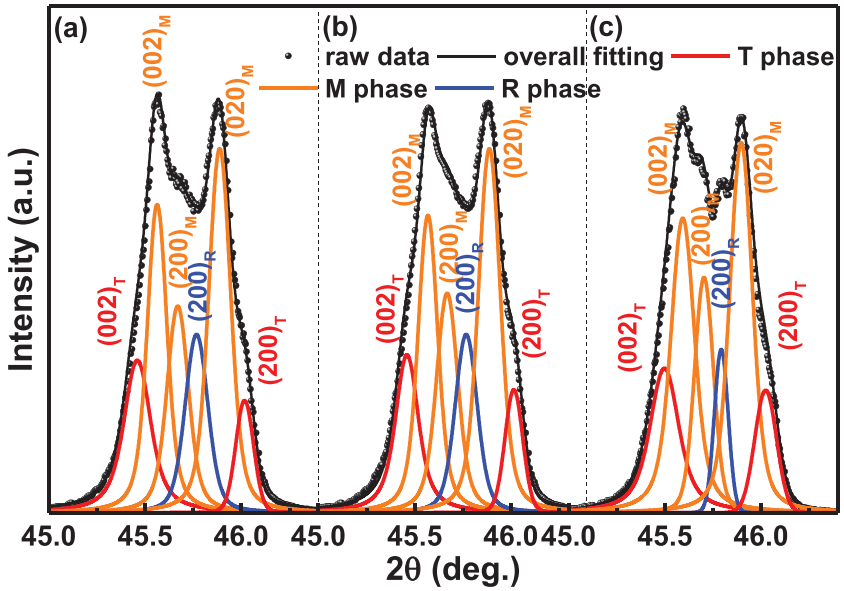

Fig. 5. The comparison of the $(200)_C$ reflection at room temperature for the poled sample (a) before thermal annealing and after thermal annealing at 60 °C for (b) 1st cycle and (c) 5th cycle derived from the conventional XRD using Cu Kα radiation (λ=1.5406 Å). One cycle stands for heating from room temperature to a certain temperature, and then remaining at this temperature for 20 min and finally cooling to room temperature for the d_{33} measurement.

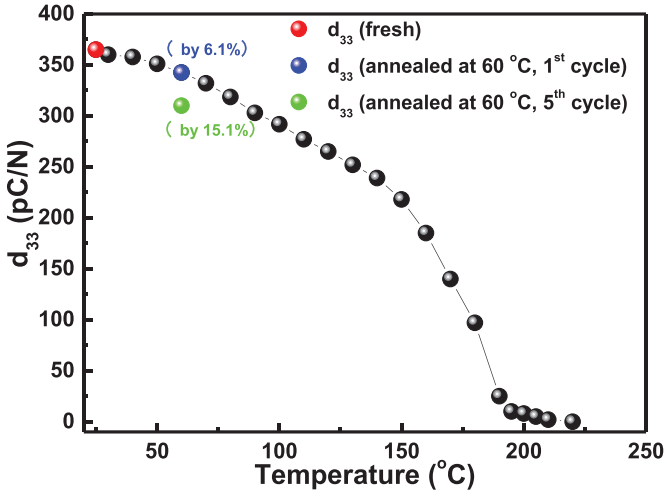

Fig. 6. The evolution of piezoelectric coefficient d_{33} under different thermal annealing conditions.

4. Discussion

From the aforementioned results, one can conclude that both unpoled and poled samples own a PPB, which should be closely attributed to the polymorphism of *R-O-T* and *R-M$_C$-T* transitions for unpoled and poled samples, respectively. For the unpoled sample, the polymorphism of *R-O* and *O-T* transitions can be easily understood, since both PPTs inherit from the NKN matrix. It seems that understanding the polymorphism of *R-M$_C$* and *M$_C$-T* transitions in poled samples still needs more analysis. Paul et al. proposed that the *O-M$_B$* and *O-M$_C$* transition can be induced under external electric fields along [001]c and [111]c directions in $BaTiO_3$ that is strikingly similar to the NKN solid solution in the phase transition sequence [42]. Vanderbilt et al. also proposed that the prototypical $KNbO_3$ can undergo *R-O-M$_A$-T* or even *R-M$_B$-O-M$_A$-T* PPT [40]. If one resurveys the phase diagram of pure NKN, the *R-O-T* and *R-M$_C$-T* PPTs observed in current work are very similar to those of pure NKN at the K-rich side and Na-rich side, respectively [7], where these two PPT sequences are linked by an *O-M$_C$* transition driven by the change of K/Na ratio. In modified NKN-based lead-free compositions, the *O-M$_C$* transition can be induced either by composition modulation, such as in some *O-T* PPB composition systems [43,44], or by external electric fields just like in the present study. This is because that *M$_C$* phase can change into *O* phase only through a slight deviation of the polarization vector from the $[101]_c$ axis along $(010)_c$ plane. According to in-situ XRD results shown in Fig. 2(a) and the E_c value from P-E curves (Fig. 3(b)), the threshold field corresponding to the *O-M$_C$* transition is as low as ~1 kV/mm. As a result, the PPT changes from the *R-O-T* sequence before poling to the *R-M$_C$-T* sequence after poling, as sketched in Fig. 4(e,f). Fig. 4(g) and (h) compare the relationship of the phase structure and the corresponding P_s vector between different phases for the studied sample before and after poling, respectively. It can be seen that the rotation of P_s during *R-O-T* PPT is discontinuous from $[111]_C$ to $[101]_C$ and finally to $[001]_C$ direction. By comparison, for the *R-M$_C$-T* sequence, although the rotation of Ps during *R-M$_C$* transition is still discontinuous due to the jump of the P_s direction from $[111]_C$ to $[u0w]_C$ ($u \neq w$), yet the Ps direction can be continuously rotated during *M$_C$-T* transition from $[u0w]_C$ to $[001]_C$ along the $(010)_C$ plane. This may induce flatter internal energy surface for the M_C-T transition than that for the R-M_C transition. As a result, the maximal piezoelectric and electromechanical properties usually appear at the T-rich side in many poled NKN-based systems [20,23].

5. Conclusions

A triple-phase coexistence rather than a two-phase coexistence has been identified in typical NKNS-LT-0.025BZ lead-free piezoelectric ceramics close to the *R-T* phase boundary at either virgin or poled samples. Ex/in-situ XRD data and P/S-E bipolar loops at different cycles suggest an electric field induced irreversible *O-M$_C$* phase transition. The experimental results clearly demonstrate the polymorphism of both *R-O-T* (virgin state) and *R-M$_C$-T* (poled state) phase transition considering the nature of temperature driven phase transition. Similar to the virgin sample, the poled sample still owns a PPB among *R*, *M$_C$* and *T*, instead of a traditional MPB. Consequently, an obvious degradation of quasi-static

piezoelectric properties occurs during repeated thermal cycling as a result of the domain de-texturing of not only M_C phase, but also *R* and *T* phases during the process of repeated temperature driven phase transition. The polarization vectors rotation of M_C-*T* transition is continuous compared with the *O*-M_C phase transition helps understand why maximal piezoelectric and electromechanical properties usually appear at the *T*-rich side in many poled NKN-based systems. The present study would provide a general route to understanding origin of temperature-sensitive piezoelectric properties from the aspect of the structural nature of multi-phase coexistence in NKN-based lead-free piezoelectric ceramics.

Declaration of Competing Interest

The authors declare that they have no known competing financial interests or personal relationships that could have appeared to influence the work reported in this paper.

Acknowledgements

This work was supported by the National Natural Science Foundation of China (Grants No. 51402079, U19A2087).

Supplementary materials

Supplementary material associated with this article can be found, in the online version, at doi:10.1016/j.actamat.2020.06.002.

References

[1] B. Jaffe, R.S. Roth, S. Marzullo, Piezoelectric properties of lead zirconate-lead titanate solid-solution ceramics, J. Appl. Phys. 25 (1954) 809.
[2] D. Damjanovic, A morphotropic phase boundary system based on polarization rotation and polarization extension, Appl. Phys. Lett. 97 (2010) 062906.
[3] R. Guo, L.E. Cross, S.E. Park, B. Noheda, D.E. Cox, G. Shirane, Origin of the high piezoelectric response in $PbZr_{1-x}Ti_xO_3$, Phys. Rev. Lett. 84 (2000) 5423–5426.
[4] R. Theissmann, L.A. Schmitt, J. Kling, R. Schierholz, K.A. Schonau, H. Fuess, M. Knapp, H. Kungl, M.J. Hoffmann, Nanodomains in morphotropic lead zirconate titanate ceramics: on the origin of the strong piezoelectric effect, J. Appl. Phys. 102 (2007) 024111.
[5] B. Jaffe, W.R. Cook, H. Jaffe, Piezoelectric Ceramics, Academic Press, New York, 1971.
[6] T. Takenaka, K. Maruyama, K. Sakata, $(Bi_{1/2}Na_{1/2})TiO_3$-$BaTiO_3$ system for lead--free piezoelectric ceramics, Jpn. J. Appl. Phys. 30 (1991) 2236–2239.
[7] D.W. Baker, P.A. Thomas, N. Zhang, A.M. Glazer, A comprehensive study of the phase diagram of $K_xNa_{1-x}NbO_3$, Appl. Phys. Lett. 95 (2009) 091903.
[8] Y. Saito, H. Takao, T. Tani, T. Nonoyama, K. Takatori, T. Homma, T. Nagaya, M. Nakamura, Lead-free piezoceramics, Nature 432 (2004) 84–87.
[9] E.K. Akdogan, K. Kerman, M. Abazari, A. Safari, Origin of high piezoelectric activity in ferroelectric $(K_{0.44}Na_{0.52}Li_{0.04})(Nb_{0.84}Ta_{0.1}Sb_{0.06)}O_3$ ceramics, Appl. Phys. Lett. 92 (2008) 112908.
[10] L. Zhang, M. Zhang, L. Wang, C. Zhou, Z. Zhang, Y.G. Yao, L.X. Zhang, D.Z. Xue, X.J. Lou, X.B. Ren, Phase transitions and the piezoelectricity around morphotropic phase boundary in $Ba(Zr_{0.2}Ti_{0.8})O_3$-$x(Ba_{0.7}Ca_{0.3})TiO_3$ lead-free solid solution, Appl. Phys. Lett. 105 (2014) 162908.
[11] R.Z. Zuo, J. Fu, D.Y. Lv, Y. Liu, Antimony tuned rhombohedral-orthorhombic phase transition and enhanced piezoelectric properties in sodium potassium niobite, J. Am. Ceram. Soc. 93 (2010) 2783–2787.
[12] Y. Tian, X.L. Chao, L. Jin, L.L. Wei, P.F. Liang, Z.P. Yang, Polymorphic structure evolution and large piezoelectric response of lead-free $(Ba,Ca)(Zr,Ti)O_3$ ceramics, Appl. Phys. Lett. 104 (2014) 112901.
[13] R.Z. Zuo, J. Fu, D.Y. Lv, Phase transformation and tunable piezoelectric properties of lead-free $(Na_{0.52}K_{0.48-x}Li_x)(Nb_{1-x-y}Sb_yTa_x)O_3$ system, J. Am. Ceram. Soc. 92 (2009) 283–285.
[14] J.G. Wu, T. Peng, Y. Wang, D.Q. Xiao, J. Zhu, Y. Jin, J.G. Zhu, P. Yu, L. Wu, Y. Jiang, Phase structure and electrical properties of $(K_{0.48}Na_{0.52})(Nb_{0.95}Ta_{0.05})O_3$-$LiSbO_3$ lead-free piezoelectric ceramics, J. Am. Ceram. Soc. 91 (2008) 319–321.
[15] R.P. Wang, H. Bando, M. Itoh, Universality in phase diagram of $(K,Na)NbO_3$-$MTiO_3$ solid solutions, Appl. Phys. Lett. 95 (2009) 092905.
[16] K. Higashide, K. Kakimoto, H. Ohsato, Temperature dependence on the piezoelectric property of $(1-x)(Na_{0.5}K_{0.5})NbO_3$-$xLiNbO_3$ ceramics, J. Eur. Ceram. Soc. 27 (2007) 4107–4110.
[17] E. Hollenstein, D. Damjanovic, N. Setter, Temperature stability of the piezoelectric properties of Li-modified KNN ceramics, J. Eur. Ceram. Soc. 27 (2007) 4093–4097.
[18] P. Zheng, J.L. Zhang, S.F. Shao, Y.Q. Tan, C.L. Wang, Piezoelectric properties and stabilities of CuO-modified $Ba(Ti,Zr)O_3$ ceramics, Appl. Phys. Lett. 94 (2009) 032902.
[19] G. Singh, V.S. Tiwari, P.K. Gupta, Thermal stability of piezoelectric coefficients in $(Ba_{1-x}Ca_x)(Zr_{0.05}Ti_{0.95})O_3$: a lead-free piezoelectric ceramic, Appl. Phys. Lett. 102 (2013) 162905.
[20] R.Z. Zuo, J. Fu, Rhombohedral-tetragonal phase coexistence and piezoelectric properties of $(NaK)(NbSb)O_3$-$LiTaO_3$-$BaZrO_3$ leadf-free ceramics, J. Am. Ceram. Soc. 94 (2011) 1467–1470.
[21] P. Li, J.W. Zhai, B. Shen, S.J. Zhang, X.L. Li, F.Y. Zhu, X.M. Zhang, Ultrahigh piezoelectric properties in textured $(K,Na)NbO_3$-based lead-free ceramics, Adv. Mater. 30 (2018) 1705171.
[22] C.M. Zhou, J.L. Zhang, W.Z. Yao, X.M. Wang, D.K. Liu, X. Sun, Piezoelectric performance, phase transitions, and domain structure of $0.96(K_{0.48}Na_{0.52})(Nb_{0.96}Sb_{0.04})O_3$-$0.04(Bi_{0.50}Na_{0.50})ZrO_3$ ceramics, J. Appl. Phys. 124 (2018) 164101.
[23] M.K. Lee, S.A. Yang, J.J. Park, G.J. Lee, Proposal of a rhombohedral-tetragonal phase composition for maximizing piezoelectricity of $(K,Na)NbO_3$ ceramics, Sci. Rep. 9 (2019) 4195.
[24] X. Lv, J.G. Zhu, D.Q. Xiao, X.X. Zhang, J.G. Wu, Emerging new phase boundary in potassium sodium-niobate based ceramics, Chem. Soc. Rev. 49 (2020) 671–707.
[25] T. Zheng, H.J. Wu, Y. Yuan, X. Lv, Q. Li, T.L. Men, C.L. Zhao, D.Q. Xiao, J.G. Wu, K. Wang, J.-.F. Li, Y.L. Gu, J.G. Zhu, S.J. Pennycook, The structural origin of enhanced piezoelectric performance and stability in lead free ceramics, Energy Environ. Sci. 10 (2017) 528–537.
[26] D.W. Wang, F. Hussain, A. Khesro, A. Feteira, Y. Tian, Q.L. Zhao, I.M. Reaney, Composition and temperature dependence of structure and piezoelectricity in $(1-x)(K1_{-y}Na_y)NbO_3$-$x(Bi_{1/2}Na_{1/2})ZrO_3$ lead-free ceramics, J. Am. Ceram. Soc. 100 (2017) 627–637.
[27] B. Orayech, A. Faik, G.A. Lopez, O. Fabelo, J.M. Igartua, Mode-cry stallography analysis of the crystal structures and the low-and high-temperature phase transitions in $Na_{0.5}K_{0.5}NbO_3$, J. Appl. Cryst. 48 (2015) 318–333.
[28] H. Mgbemere, G. Schneider, M. Hoelzel, M. Hinterstein, Neutron diffraction study of $(K_xNa_{1-x})NbO_3$-based ceramics from low to high temperatures, J. Appl. Cryst. 49 (2016) 891–901.
[29] K. Yan, S. Ren, M.X. Fang, X.B. Ren, Crucial role of octahedral untilting R3m/P4mm morphotropic phase boundary in highly piezoelectric perovskite oxide, Acta Mater 134 (2017) 195–202.
[30] R.P. Wang, K. Wang, F.Z. Yao, J.F. Li, F.H. Schader, K.G. Webber, W. Jo, J. Rodel, Temperature stability of lead-free niobite piezoceramics with engineered morphotropic phase boundary, J. Am. Ceram. Soc. 98 (2015) 2177–2182.
[31] C.L. Zhao, J. Yin, Y. Huang, J.G. Wu, Polymorphic characteristics challenging electrical properties in lead-free piezoceramics, Dalton T 48 (2019) 11250–11258.
[32] P. Li, Y. Huan, W.W. Yang, F.Y. Zhu, X.L. Li, X.M. Zhang, B. Shen, J.W. Zhai, High--performance potassium-sodium niobite lead-free piezoelectric ceramics based on polymorphic phase boundary and crystallographic texture, Acta Mater 165 (2019) 486–495.
[33] T.K. Lee, D.H. Kim, S.H. Cho, J.S. Kim, J. Ryu, C.W. Ahn, T.H. Lee, G.H. Kim, S. Nahm, Pseudocubic-based polymorphic phase boundary structures and their effect on the piezoelectric properties of $(Li,Na,K)(Nb,Sb)O_3$-$SrZrO_3$ lead-free ceramics, J. Alloys Compd 784 (2019) 1334–1343.
[34] J. Fu, R.Z. Zuo, S.C. Wu, J.Z. Jiang, L. Li, T.Y. Yang, X.H. Wang, L.L. Li, Electric field induced intermediate phase and polarization rotation path in alkaline niobite based piezoceramics close to the rhombohedral and tetragonal phase boundary, Appl. Phys. Lett. 100 (2012) 122902.
[35] R.Z. Zuo, J. Fu, S.B. Lu, Z.K. Xu, Normal to relaxor ferroelectric transition and domain morphology evolution in $(K,Na)(Nb,Sb)O_3$-$LiTaO_3$-$BaZrO_3$ lead-free ceramics, J. Am. Ceram. Soc. 94 (2011) 4352–4357.
[36] K. Xu, J. Li, X. Lv, J.G. Wu, X.X. Zhang, D.Q. Xiao, J.G. Zhu, Superior piezoelectric properties in potassium-sodium niobite lead-free ceramics, Adv. Mater. 28 (2016) 8519–8523.
[37] Q. Liu, Y.C. Zhang, J. Gao, Z. Zhou, H. Wang, K. Wang, X.W. Zhang, L.T. Li, J.F. Li, High-performance lead-free piezoelectrics with local structural heterogeneity, Energy Environ. Sci. 11 (2018) 3531–3539.
[38] Y.L. Qin, J.L. Zhang, W.Z. Yao, C.J. Lu, S.J. Zhang, Domain configuration and thermal stability of $(K_{0.48}Na_{0.52})(Nb_{0.96}Sb_{0.04})O_3$-$Bi_{0.50}(Na_{0.82}K_{0.18})_{0.50}ZrO_3$ piezoceramics with high d_{33} coefficient, ACS Appl. Mater. Interfaces 8 (2016) 7257–7265.
[39] B.H. Toby, R.B. Von Dreele, GSAS-II: the genesis of a modern open-source all purpose crystallography software package, J. Appl. Crystallogr. 46 (2013) 544–549.
[40] D. Vanderbilt, M.H. Cohen, Monoclinic and triclinic phases in higher-order Devonshire theory, Phys. Rev. B 63 (2001) 094108.
[41] J. Fu, R.Z. Zuo, X.Y. Gao, Electric field induced monoclinic phase in $(Na_{0.52}K_{0.48})(Nb_{1-y}Sb_y)O_3$ ceramics close to the rhombohedral-orthorhombic polymorphic phase boundary, Appl. Phys. Lett. 103 (2013) 182907.
[42] Paul, T. Nishimatsu, Y. Kawazoe, U.V. Waghmare, Polarization rotation, switching, and electric-field-temperature phase diagrams of ferroelectric $BaTiO_3$: a molecular dynamics study, Phys. Rev. B 80 (2009) 024107.
[43] W.W. Ge, Y. Ren, J.L. Zhang, C.P. Devreugd, J.F. Li, D. Viehland, A monoclinic-tetragonal ferroelectric phase transition in lead-free $(K_{0.5}Na_{0.5})NbO_3$-x%$LiNbO_3$ solid solution, J. Appl. Phys. 111 (2012) 103503.
[44] T.A. Skidmore, T.P. Comyn, A.J. Bell, F.Y. Zhu, S.J. Milne, Phase diagram and structure-property relationships in the lead-free piezoelectric system: $Na_{0.5}K_{0.5}NbO_3$-$LiTaO_3$, IEEE Trans. Ultrason. Ferroelectr. Freq. Control 58 (2011) 1819–1825.